A Modified Carrier-Based Advanced Modulation Technique for Improved Switching Performance of Magnetic Linked Medium Voltage Converters

Md. Ashib Rahman, *Member*, *IEEE*, Md. Rabiul Islam, *Senior Member*, *IEEE*, Kashem M. Muttaqi, *Senior Member*, *IEEE* , Youguang Guo, *Senior Member*, *IEEE*, Jianguo Zhu, *Senior Member*, *IEEE*, Danny Sutanto, *Senior Member*, *IEEE*, and Gang Lei, *Member*, *IEEE*

***Abstract*—The high-frequency magnetic link is gaining popularity due to its light weight, small volume, and inherent voltage balancing capability. Those features can simplify the utilization of multilevel converter (MLC) for the integration of renewable energy sources to the grid with compact size and exert economic feasibility. The modulation and control of MLC are crucial issues especially for grid connected applications. To support the grid, the converter may need to operate in over-modulation (OVM) region for short periods depending upon the loading conditions. This OVM operation of the converter causes increased harmonic losses and adverse effects on overall system efficiency. On top of that, the size and cost of filtering circuitry become critical to eliminate the unwanted harmonics. In this regard, a modified OVM scheme with phase disposed carriers for grid connected high frequency magnetic link-based cascaded H-bridge (CHB) MLC is proposed for the suppression of harmonics and the reduction of converter loss. Furthermore, with the proposed OVM technique, the voltage gain with modulation index can be increased up to the range, which is unlikely to be achieved using the classical ones. Extensive simulations are carried out with a 2.24 MVA permanent magnet synchronous generator-based wind energy conversion system, which is connected to the 11 kV ac grid through a high-frequency magnetic link and a 5-level CHB MLC. A scaled down laboratory prototype is implemented to validate the performance of the converter.**

***Index Terms*—Medium voltage multilevel converter, over modulation technique, grid connection, high-frequency magnetic link, wind energy.**

I. Introduction

WIND energy harnessing technology is becoming popular and mature day by day as a potential renewable energy source. It is estimated that the global capacity of wind energy installation will reach up to 104 GW by 2025 [1]. Stand-alone and hybrid wind energy based systems have been gaining popularity nowadays for remote area power supply systems [2]. Although the power capacity of wind turbine generators has increased to the megawatt range, the voltage rating of most generators is still limited to 690 V. Therefore, a heavy and bulky oil-filled transformer is commonly used to step up the voltage from 690 V to 33 kV transmission voltage. For small-scale wind power generation, fully rated voltage source converter coupled permanent magnet synchronous generator (PMSG) based wind energy conversion system is suitable for its inherent efficiency and reliability [3]. PMSG ensures complete decoupled operation from the system frequency and wider rotor speed range to have better frequency response [4]. Moreover, this type of system offers higher torque at low speed without the requirement of separate excitation current supply. In this regard, the multilevel converter (MLC) coupled PMSG setup is chosen in this work.

The MLC topology has the potential to operate in transformer and filter less system, and it can reduce the size of overall converter to 50–70% [5]. They are becoming industry standard to replace the classical two-level converters having 2.3–30 kV, 0.3–32 MVA power ratings, and better candidates for the operation of medium (0.1–5.0 MW) to large scale (6.0–50 MW) micro-grid system [6]. In this paper, the cascaded H-bridge (CHB) converter is considered for its superior qualities and higher rating, (the maximum rating is 13.8 kV, 1400 A, and 31.0 MVA [7]–[9]).

Grid connected converters are normally operated in the linear modulation mode. In some cases, when a sudden over-rated load is applied to the grid or in case of power imbalance, line voltage tends to decrease. Also, the grid side current regulator increases the reference voltage for increased voltage gain to keep the line voltage constant. This can lead the modulator to operate in the over-modulation (OVM) region. This article focuses on the converter overall loss and total harmonic distortion (THD) reduction in the OVM region in comparison with the existing OVM techniques. The fundamental voltage gain increases linearly with the increase of modulation index (MI) in the linear modulation mode and the opposite is true in the case of regular OVM techniques. The traditional OVM technique possesses some adverse effects on converters, such as: (1) generation of sub-carrier

Manuscript received, August 13, 2018; revised October 2, 2018.

M. A. Rahman, M. R. Islam, K. M. Muttaqi, and D. Sutanto are with the School of Electrical, Computer and Telecommunications Engineering, University of Wollongong, NSW 2522, Australia. E-mails: mar997@uowmail.edu.au, mrislam@uow.edu.au, kashem@uow.edu.au, soetanto@uow.edu.au.

Y. G. Guo, J. G. Zhu, and G. Lei are with the Faculty of Engineering and Information Technology, University of Technology Sydney, NSW 2007, Australia. E-mails: youguang.guo-1@uts.edu.au, jianguo.zhu@uts.edu.au.

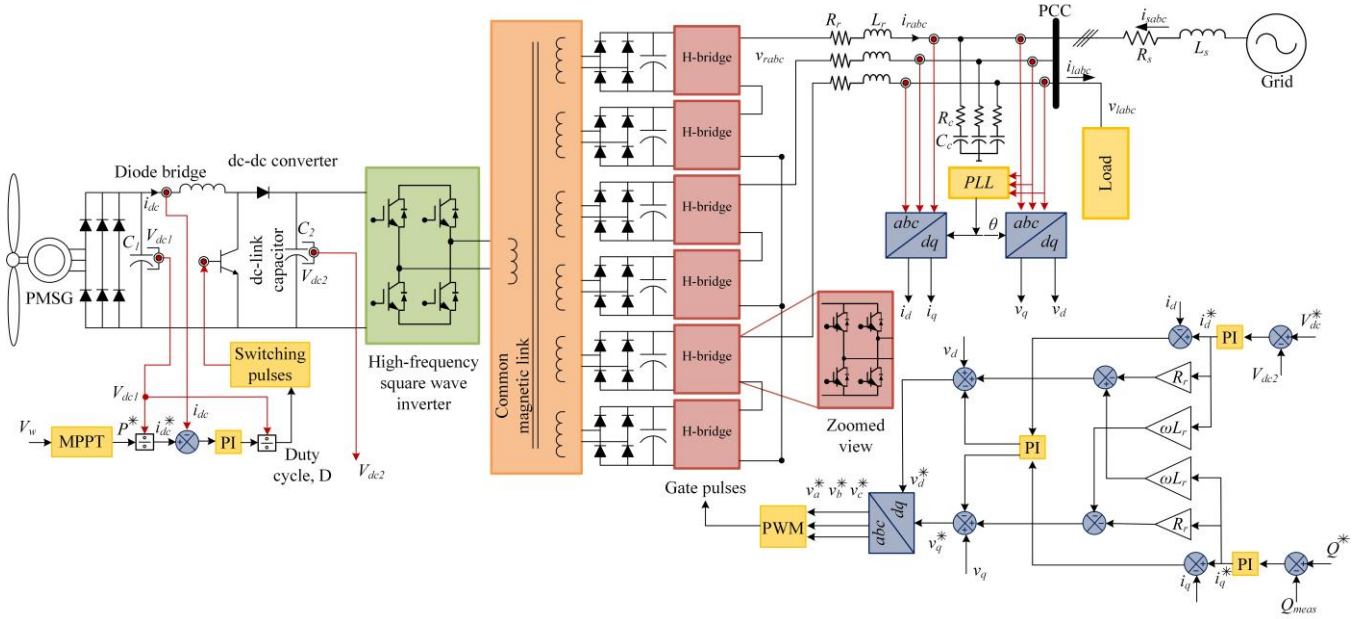

Fig. 1. Control scheme for high-frequency magnetic link coupled, five-level cascaded H-bride converter-based grid-connected wind energy conversion system.

harmonic in the converter output voltage and current (low level base-band distortion); (2) gain reduction of fundamental voltage component; (3) breaking down linearity of fundamental voltage with MI; and (4) abrupt dropping of switch pulses. These properties make the OVM technique avoidable in the normal mode of converter operation. However, in OVM, the fundamental voltage component can be increased within a reasonable limit, which can help the converters and variable speed drives to utilize the full rated power, exhibit reliable performance at the time of voltage deviation of the dc bus, and reduce the overall converter cost [11]. Moreover, the modulator needs to operate in the OVM region to compensate the voltage fluctuation or over-speed operation for brief period in drives and traction applications [12]. The OVM has been utilized in hybrid 1.575 GW rated MLC for fault tolerant operation [13] and high-voltage direct current applications [14]. The OVM mode has also been applied in hybrid MLC [15] and matrix converters to improve the voltage transfer ratio and to reduce low frequency voltage harmonics [16], [17].

The OVM method is investigated with several bus-clamped pulse width modulation (BCPWM) schemes as shown in Fig. 2, which shows the linearity property with MI less than or equal to 0.907. The main advantage of utilizing these pulse width modulation (PWM) schemes include 33% less switching loss than the regular PWM methods [18] and reduced harmonic distortion than the regular space vector PWM (SVPWM) schemes in the OVM region. Recently, the third harmonic injected 60° BCPWM (THSDBCPWM) method is introduced to show better harmonic spectra compared to the other conventional PWM methods [19].

The OVM method is analyzed for the neutral point clamped converter (NPC) [20] and the modular multilevel converter (MMC) [21]–[25]. In [20], a modulation method is proposed to keep the dc-link voltage of the NPC converter constant during the OVM operation by injecting biasing or offset signals. The method offers fundamental voltage gain reduction with additional switching losses. Although, the optimal design parameters of the full-bridge MMC [21] and the arm voltage balancing strategy of the half-bridge MMC [22] under the OVM region are investigated, but no distortion or loss scenario is reported. BCPWM or zero sequence injection techniques are applied to MMC in OVM to reduce capacitor voltage ripples and switching losses with additional closed loop controller [23], and to balance submodule arm currents [24] without mentioning energy loss profile.

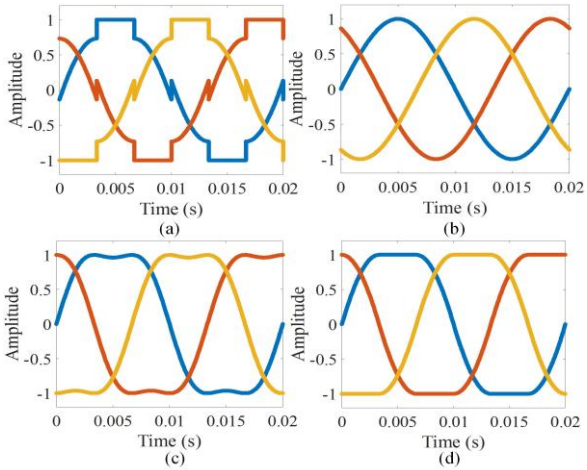

Fig. 2. Different modulating signals: (a) sinusoidal 60° bus-clamped signal, (b) pure sinusoidal signal, (c) third harmonic injected signal, and (d) third harmonic injected 60° bus-clamped signal.

It is to be noted, however, that all of the previously mentioned techniques have taken the advantage of utilizing different offset or zero sequence signals corresponding to the modulating signals for operating the converter in a larger modulation range and fulfilling some stability requirements. A comprehensive literature review shows that a technique using carrier signal modifications have not been reported so far. In a

multilevel converter, multiple isolated dc voltage supplies are required, which poses complexity in the voltage balancing control. The high-frequency magnetic link has the capability to generate isolated and balanced dc sources without any control complexities [10] and solve the dc-link voltage unbalance problem. Moreover, the proposed new topology, as shown in Fig. 1 makes the energy conversion system compact, lightweight, and cost effective.

In this paper, a new carrier signal based OVM technique for full-bridge MMC is utilized if the converter goes into the OVM mode for a short period due to the unwanted loading conditions. Here, along with the zero sequence injecting signal, a carrier modification is implemented to obtain the optimum outcome in terms of distortion, loss and voltage gain. The proposed technique can reduce the converter loss and keep the voltage gain approximately constant in comparison with the exiting OVM techniques by modifying the carrier amplitude with four types of PWM schemes: the sinusoidal PWM (SPWM), third harmonic injected PWM (THPWM), THSDBCPWM, and sinusoidal 60° BCPWM (SSDBCPWM) [25]. This paper is the extended version of [25] with high-frequency magnetic link-based grid integrated system, synchronous frame-based controller design, and inclusion of experimental investigation.

II. Traditional Overmodulation Techniques

Earlier OVM techniques are commonly investigated for two or three-level converters with SVPWM. MI is the basic parameter to measure the gain scenario of any PWM strategy. For a two-level converter, MI can be defined as shown in (1), where $V_{f(peak)}$ is the inverter line to neutral fundamental peak voltage, V_{dc} the input dc voltage, and m the amplitude modulation index (AMI) between the modulating and carrier signals. The term $2V_{dc}/\pi$ is the highest voltage gain achievable and is termed as the six-step mode voltage.

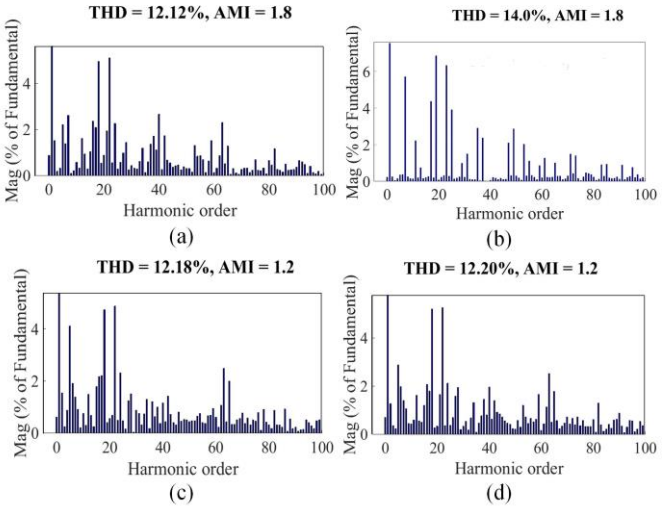

Fig. 3. Harmonic distortion for different modulations in regular OVM mode: (a) SPWM, (b) SSDBCPWM, (c) THPWM, and (d) THSDBCPWM.

With this reference, the highest MI in the linear modulation region is 0.907.

$$M_i^{2L} = \frac{mV_{f(peak)}}{\frac{2V_{dc}}{\pi}} \tag{1}$$

However, for the multilevel CHB converter, (i.e. for L-level converter), the situation shown in (1) changes. The CHB MLC exhibits symmetrical square wave as the highest gain in the line to neutral voltage, instead of the six-step voltage for two-level case. The modified equation to calculate M_i for L level CHB converter can be given as,

$$M_i^{MLC} = \frac{mV_{f(peak)}}{\frac{4}{\pi}\left(\frac{L-1}{2}\right)V_{dc}} \tag{2}$$

where V_{dc} is the cell voltage of (L-1)/2 cells for single phase.

Although the definitions of M_i in (1) and (2) look different, the values would be the same because the fundamental component of CHB MLC will increase with the increase of H-bridge cells. For example, for sinusoidal PWM, the peak of fundamental component of L level CHB converter will be $V_{dc}(L\text{-}1)/2$. This results in the same MI value for both two-level and multilevel converters.

III. Proposed Phase Disposition PWM in Over-Modulation Region

For the L level converter, the L–1 carrier signals have equal amplitude and frequency without any amplitude band gap among them in the case of regular phase disposition PWM (PDPWM). When the ratio m tends to become higher than unity, the regular OVM mode starts. Fig. 3 demonstrates the overall THD scenario of different modulators, where m is chosen as 1.8 for SPWM and SSDBCPWM, and 1.2 for THPWM and THSDBCPWM. With these values, the modulation techniques offer the lowest percentage of THD.

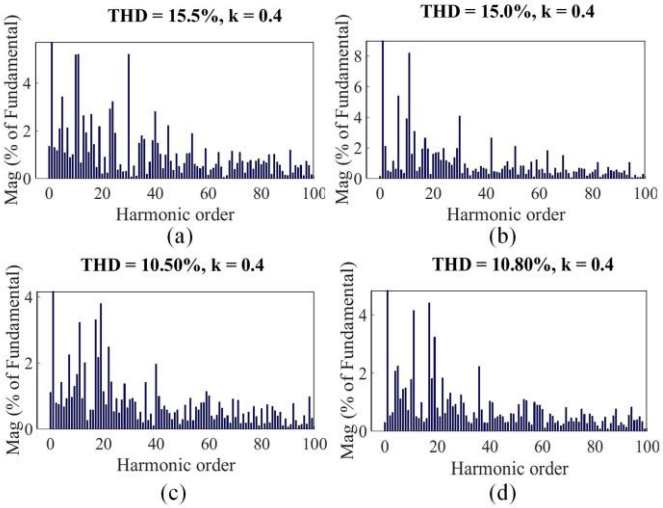

Fig. 4. Percentage THD of different modulation techniques in the proposed OVM mode: (a) SPWM, (b) SSDBCPWM, (c) THPWM, and (d) THSDBCPWM.

To improve the THD performance and loss characteristics of the converter in the OVM region, the peak of the carrier signals is decreased, unlike the case of regular PDPWM. Therefore, an amplitude band gap is introduced among the carrier signals. In this way, the OVM mode starts with fixed modulating signal amplitude. Consequently, the carrier signal amplitude can be calculated as,

$$A_{cr} = \frac{kA_r}{L-1} \tag{3}$$

where $k \in \mathbf{R}$ and $0 < k < 1$. The dc offset parameters are added with A_{cr} for the contiguity. The harmonic profiles with the modified technique are shown in Fig. 4. The band gap B_{cr} between the two carrier signals is

$$B_{cr} = \frac{(1-k)A_r}{L-1} \tag{4}$$

The dc offset parameters can be calculated by

$$F_n = \left(\frac{A_r}{2}\right)\frac{L-2n}{L-1} \tag{5}$$

where $n = 1, 2, 3, \ldots (L-1)/2$. In this work, the target reference normalized peak is chosen as 1.0 and different k exhibits different modulation indices, THD and fundamental voltage values. As the peak to peak amplitude of the carrier will decrease with the increase of k, the modified amplitude modulation index m_n for a given value of A_r, can be determined by

$$m_n = \frac{L-1}{L+k-2} \tag{6}$$

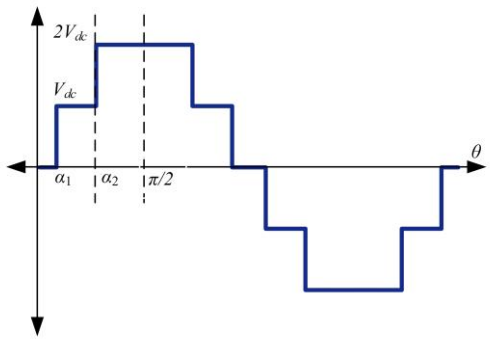

Fig. 5. Output phase voltage of five-level converter for $k = 0$.

In this way, the highest fundamental gain with the proposed OVM technique can be achieved when k becomes zero. The output phase voltage of the converter becomes staircase signal as shown in Fig. 5 for the five-level case. The signal is square wave symmetric and the *Fourier series* of this type of signal can be expressed as,

$$V(\theta) = V_x(\alpha_i)\sin(x\theta) \tag{7}$$

where x is the harmonic order, V_x the magnitude of the xth harmonic, α_i the step change angle of the signal, and $0 \le \alpha_i \le \pi/2$ (i = 1, 2, ……. (L-1)/2). Due to the quarter wave symmetric property, the even order harmonics will not appear in the signal. The odd order harmonic magnitudes can be calculated by

$$V_x(\alpha) = \frac{4V_{dc}}{x\pi}\sum_{i=1,3,5\ldots}^{(L-1)/2}\cos(x\alpha_i) \tag{8}$$

From (8), the fundamental component of L level converter output voltage can be easily obtained. However, this type of staircase signal contains the highest low order harmonic components, which are totally unwanted. In this case, an optimized value of k should be chosen, so that the harmonics remain lower than the classic OVM techniques and the gain can be increased.

IV. Loss Analysis of Multilevel Converter in Over-modulation Region

An optimized modulation method should exhibit low loss, low THD and high voltage gain. To demonstrate the superiority of the proposed OVM technique, this section covers the loss analysis of the multilevel converter. Commercially produced insulated gate bipolar transistor (IGBT) comes with IGBT switch and antiparallel diode. IGBT has conduction loss $P_{avgC,T}$, switch-on loss $P_{switchT,on}$, and switch-off loss $P_{switchT,off}$. Diode only shows switch-off $P_{switchD,off}$ and conduction loss $P_{avgC,D}$. $P_{avgC,T}$ and $P_{avgC,D}$ can be determined as,

$$P_{avgC,T} = v_{ce0,T}I_{avgC,T} + R_{ce,T}I^2_{rmsC,T} \tag{9}$$

$$P_{avgC,D} = v_{ce0,D}I_{avgC,D} + R_{ce,D}I^2_{rmsC,D} \tag{10}$$

where subscripts T and D stand for transistor and diode, v_{ce} and i_c denote the collector-emitter voltage and collector current, I_{avgC} and I_{rmsC} are the average and rms collector currents, respectively, V_{ce0} is the zero-current voltage, and R_{ce} the collector-emitter resistance. These values can be obtained from the device datasheet characteristics curve. The transistor and diode switch on and off losses can be calculated as,

$$P_{switchT,on} = \frac{1}{T}\frac{v_{ce,off}(t)}{v_{ce,ref}}\sum_{j=1}^{N_{T,on}}[E_{T,on(j)}(i_C(t))] \tag{11}$$

$$P_{switchT,off} = \frac{1}{T}\frac{v_{ce,off}(t)}{v_{ce,ref}}\sum_{j=1}^{N_{T,off}}[E_{T,off(j)}(i_C(t))] \tag{12}$$

$$P_{switchD,off} = \frac{1}{T}\frac{v_{D,off}(t)}{v_{ce,ref}}\sum_{j=1}^{N_{D,off}}[E_{D,off(j)}(i_D(t))] \tag{13}$$

where $v_{ce,off}$ and $v_{D,off}$ are the blocking voltages with reference blocking voltage $v_{ce,ref}$. The switching loss energies $E_{T,on}$, $E_{T,off}$, and E_{Doff} are obtained from the data sheet for instantaneous collector current.

V. Voltage Source Converter Control for Grid Synchronization

In the usual operation of converter based PMSG wind energy conversion system, the rotor blades of turbine in the turbine drive train capture the wind energy. This energy is fed

to the generator for conversion from mechanical to electrical energy. The main control objective in this case is to extract optimum power by using the optimum torque and optimum rotor speed. Furthermore, a dc-dc booster should be utilized to regulate the dc output voltage at the desired level even for varying the input voltage and output load. In this paper, an optimization technique for torque and a booster controller [26] is designed to produce optimum power from the generator and keep the dc-link voltage constant respectively.

For the synchronization and control, the synchronously rotating reference frame-based control technique with grid voltage and current as reference is adopted in this work. The characterization of the point of common coupling (PCC) voltage can be determined by

$$v_{ra} = R_r i_{ra} + L_r \frac{d}{dt}(i_{ra}) + v_{la} \tag{14}$$

$$v_{rb} = R_r i_{rb} + L_r \frac{d}{dt}(i_{rb}) + v_{lb} \tag{15}$$

$$v_{ra} = R_r i_{rc} + L_r \frac{d}{dt}(i_{rc}) + v_{lc} \tag{16}$$

After transforming the *abc* reference frame parameters to the *dq* reference frame, (14)–(16) can be expressed in the matrix form as,

$$\begin{bmatrix} v_{rd} - v_{ld} \\ v_{rq} - v_{lq} \end{bmatrix} = \begin{bmatrix} R_r + L_r \frac{d}{dt} & -\omega L_r \\ \omega L_r & R_r + L_r \frac{d}{dt} \end{bmatrix} \begin{bmatrix} i_{rd} \\ i_{rq} \end{bmatrix} \tag{17}$$

The real and reactive current *dq* components i_{rd} and i_{rq}, can control the active and reactive power transfer between grid and wind energy generation system.

TABLE I
LOSS COMPARISONS OF REGULAR AND PROPOSED PDPWM IN OVM MODE

Category PWM	Type	Switching loss (kW)	Conduction loss (kW)	Total loss (kW)	THD (%)
SPWM	m = 1.8	1.68	9.53	11.21	12.12
	k = 0.4	0.23	7.59	7.82	15.00
SDBCPWM	m = 1.8	2.57	9.43	12.00	14.00
	k = 0.4	0.52	6.62	7.14	15.50
THPWM	m = 1.2	1.66	9.55	11.21	12.18
	k = 0.4	1.50	9.37	10.87	10.50
THSDBCPWM	m = 1.2	1.66	9.51	11.17	12.20
	k = 0.4	1.51	9.31	10.82	10.80

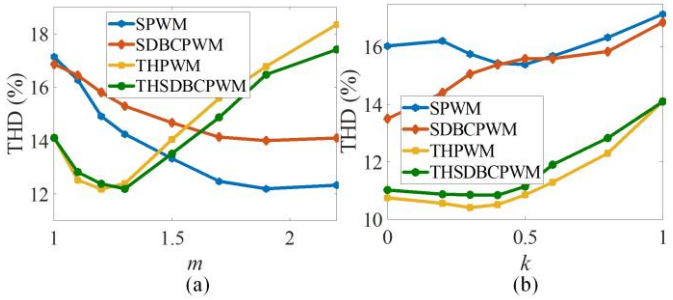

Fig. 6. THD in OVM region: (a) regular and (b) proposed methods.

In the synchronously rotating frame, it is customary to use the proportional-integral (PI) controller with the following dynamics for current controller:

$$v_{rd} = v_{ld} - \omega L_r i_{rq} + K_{pc} e_d + K_{ic} \int_0^t e_d dt \tag{18}$$

$$v_{rq} = v_{lq} - \omega L_r i_{rd} + K_{pc} e_q + K_{ic} \int_0^t e_q dt \tag{19}$$

where $e_d = i_{rdref} - i_{rd}$ and $e_q = i_{rqref} - i_{rq}$. The gains K_{pc} and K_{ic} should be chosen to minimize the cross-coupling effect between *d* and *q* current components. Supply of active power, P_r and reactive power, Q_r into the grid can be calculated by

$$P_r = \frac{V_r V_l}{Z_r} \sin(\varphi) \tag{20}$$

$$Q_r = -\frac{V_l^2}{Z_r} + \frac{V_r V_l}{Z_r} \cos(\varphi) \tag{21}$$

where V_r and V_l are the converter side voltage and line voltage, respectively, with φ defines the phase voltage angle. Therefore, the converter output voltage and power angle regulate the active and reactive power injection. The PCC voltage is controlled through an anti-windup PI controller based on the reference reactive current signal, i_{rqref} as follows,

$$i_{rqref} = K_{pc} e_l + K_{ic} \int_0^t e_l dt - K_{ic} \left(K_{rl} \left(i_{rqref} - i_s \right) \int_0^t e_l dt \right) \tag{22}$$

where $e_l = v_{l,ref} - V_l$, i_s is the output saturated current, and K_{rl} the feedback gain, which prevents the controller from going into saturation.

VI. SIMULATION RESULTS AND DISCUSSIONS

A. Simulation of Cascaded H-Bridge Multilevel Converter for Loss Evaluation in Islanded Operation

For switching and conduction loss calculation, an 11 kV, 2.4 MVA CHB five-level converter is chosen with H-bridge cell input voltage of 4 kV. IGBT Module 5SNA 0750G6503000 (6.5 kV, 750 A) of ASEA Brown Boverie (ABB) fulfills the switching purposes of the converter. The converter is simulated under 1.0 kHz switching frequency and the temperature of operation is assumed as 125 °C. Firstly, the characteristic curves from the manufacturer data sheets are approximated [19]. Then, by using (9)–(13), the switching and conduction losses are calculated. Table I summarizes the losses associated with different types of modulation techniques in the regular and proposed OVM techniques. Table I reveals that in all modulation techniques, the total loss is reduced and THD becomes lower for THPWM and THSDBCPWM in the case of the proposed one. Fig. 6 shows that decreased *k* will ensure lower THD. With the limited OVM region with the proposed technique, the approximately constant fundamental voltage of the converter refers to a very special property as shown in Fig. 7. The fundamental gain gradually decreases with the regular OVM technique as shown

in Fig. 8(a). However, the proposed technique not only keeps the gain approximately constant but also increases the gain as referred to Fig. 8(b).

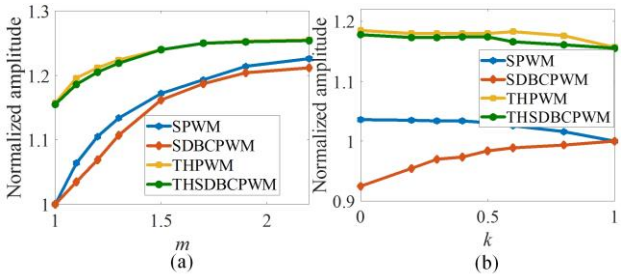

Fig. 7. Fundamental voltage (normalized) in OVM region: (a) regular and (b) proposed methods.

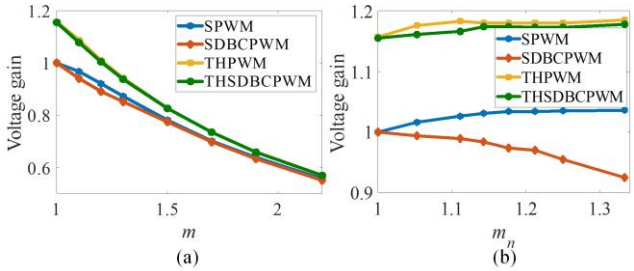

Fig. 8. Fundamental voltage gain in OVM region: (a) regular and (b) proposed methods.

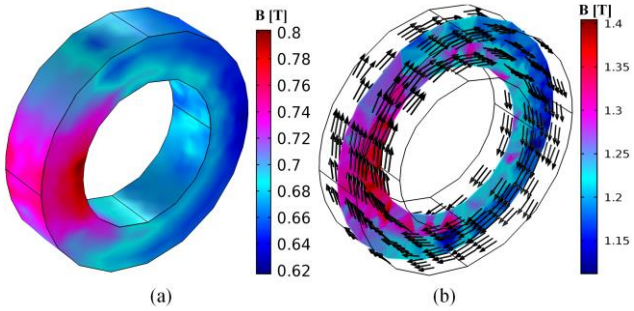

Fig. 9. (a) Simulated flux distribution of the high frequency magnetic link (primary winding excitation) and (b) single slice presentation of the direction of flux distribution.

B. Simulation of High Frequency Magnetic Link

By using the COMSOL Multiphysics software, finite element analysis is carried out to simulate the high-frequency magnetic core. Amorphous material from Metglas is selected as the core material, and the primary and secondary windings are considered as homogeneous multi-turn. The primary winding is excited with 10 kHz square wave voltage to get the flux density around 0.8 T at 0.05s as shown in Fig. 9(a). Fig. 9(b) demonstrates the slice view with the associated flux distribution directions at 0.03s.

C. Simulation of Grid Connected Wind Energy Conversion System with High Frequency Magnetic Link in Steady State

A 2 MW, 690 V PMSG based grid connected wind energy system is simulated in MATLAB/Simulink platform. The overall system with the controller architecture is shown previously as in Fig. 1. It should be noted that the system is operated to fulfill unity power factor operation in the rated condition and reaches the steady state at 0.3 s. For the drive train, a two-mass model is assumed which will run the generator with optimum rotor speed to generate optimum torque. At a particular wind velocity, the pitch regulator (not shown in Fig. 1) will sense the converter output power and rotor speed to generate optimum pitch angle, which in turn generates the optimal mechanical output from the generator. The parameters for the simulation are shown in Table II.

TABLE II
SIMULATION PARAMETERS OF PERMANENT MAGNET SYNCHRONOUS GENERATOR, CONVERTER, AND HIGH FREQUENCY MAGNETIC LINK

Wind turbine and drive train	
Optimum co-efficient	1.67×10^{-3} Nm/(rad/s)^2
Density of air	1.225 kg/m^3
Base wind speed	12 m/s
Permanent magnet synchronous generator	
Rated system power	2.24 MVA
Mechanical output power	2 MW
Rated line voltage	690 V
Rated stator current	1867.76 A
Rated rotor speed	2.356 rad/s
Number of pole pairs	30
Rated mechanical torque	852.77 kN.m
Rated rotor flux linkage	4.696 Wb
Stator winding resistance	0.73051 mΩ
Stator winding inductance	2.60 mH
High frequency magnetic link	
No. of primary winding	1
No. of secondary winding	6
Winding resistance	0.01 (p.u.)
Winding leakage inductance	3×10^{-4} (p.u).
Link operation frequency	10 kHz
Cascaded H-bridge multilevel converter	
Input cell voltage	4.0 kV
Switching frequency	1000 Hz
Filter reactive power capacity	10% of nominal power
Inductance and resistance	4.53 mH and 0.142 Ω
Main grid	
Line voltage	11 kV
Line frequency	50 Hz
Grid inductance and resistance	2.25 mH and 0.07 Ω
Short circuit ratio	7

The dc-link voltage is maintained constant by controlling the switch pulses. The dc output is fed to the high-frequency inverter to generate high-frequency square waves to feed the high-frequency magnetic link. The link will generate six isolated and balanced dc supplies after rectification for the 5-level CHB inverter. The output voltage is then fed to the grid. Normally, the grid connected converter operates under linear modulation region. In this region, the performance of the overall system in normal mode of operation is shown in Fig. 10, which reveals that the system delivers rated active power, zero reactive power with constant dc-link voltage. It can be seen from Fig. 10(a) that the active and reactive current components are completely decoupled.

To observe the performance of the converter in OVM region, at time 0.33 s, a certain extra load is added to the system and is kept connected until 0.37 s. If the load is sufficient enough to break the voltage supporting capacity of the modulator in linear modulation region, the modulator goes into the OVM region to support the grid voltage. Fig. 11

shows how carrier signals are modified in the OVM condition to decrease the converter loss and THD.

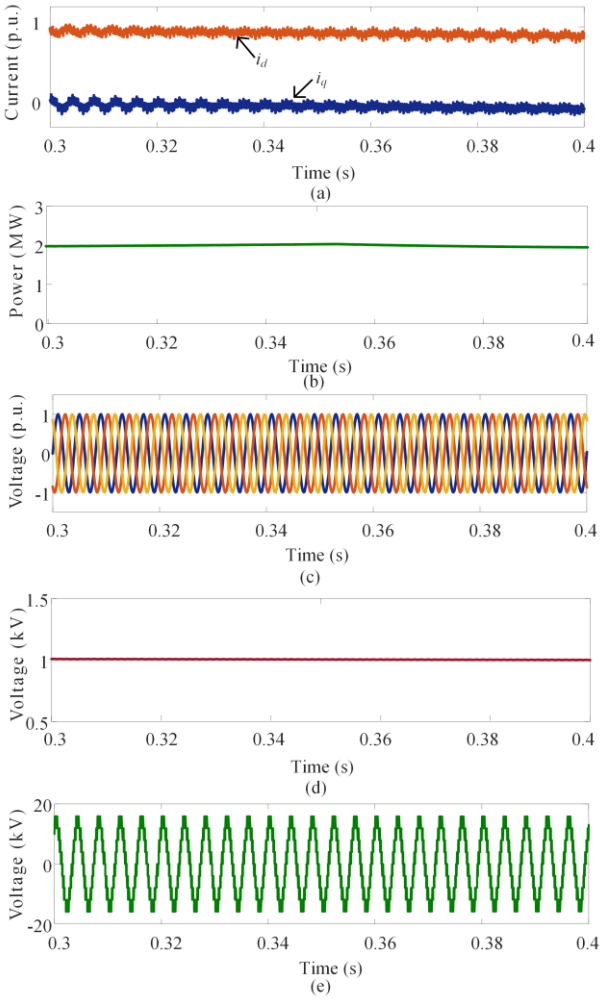

Fig. 10. Simulated performance of the system: (a) *dq* current components, (b) rated output power, (c) line voltage, (d) dc-link voltage, and (e) converter side line voltage.

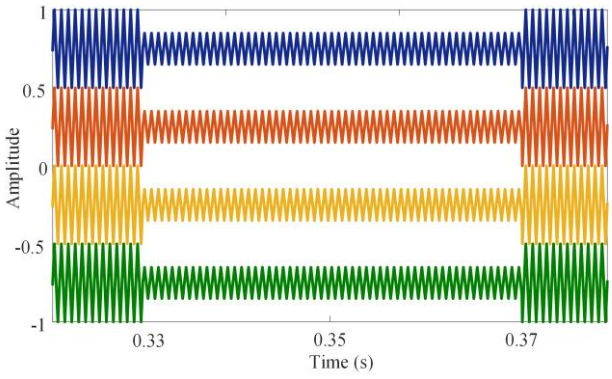

Fig. 11. Carrier signal modification to go from linear modulation to OVM mode (frequency is deliberately reduced to have better view).

Fig. 12(a) shows the *dq* current components. Fig. 12(b) shows the OVM region, where PCC voltage gets distorted in the OVM region, as shown in Fig. 12(c). Higher distortion is obtained in the OVM region than the linear region as expected. Fig. 12(d) exhibits the line currents both in linear and OVM mode where THD is measured as 4.0%. Fig. 12(e) demonstrates that dc-link voltage does not change in the OVM operation. Thorough comparisons are made among the converter output line voltages with different modulation techniques in both linear and OVM region as shown in Fig.13. It should be noted that although the line voltage THD gets higher in linear modulation than that in the OVM region, the lower order harmonics get higher in the OVM scenario, which puts extra burden on the passive filtering circuitry (weighted THD measurement can reflect this concept where lower order harmonics are highly weighted). Therefore, the controller should be back to the linear modulation mode as soon as possible for the desired output.

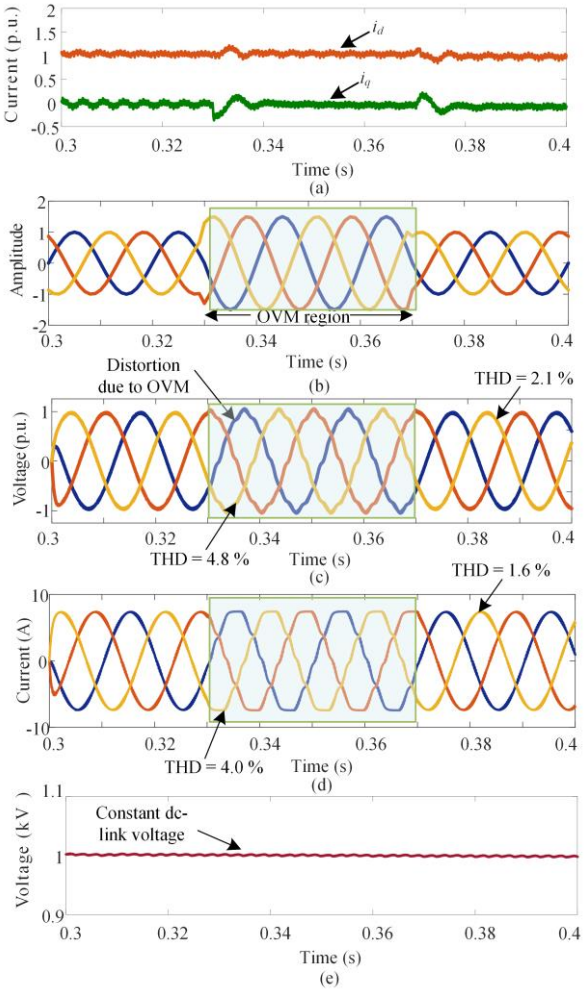

Fig. 12. Simulated performance of the system after load inclusion for sinusoidal PWM: (a) *dq* current components, (b) output reference signals from the controller, (c) line voltage (after filter), (d) line current (after filter), and (d) dc-link voltage.

For the loss calculation in the grid connected mode, the linear modulation and OVM scenario are considered separately where OVM exists for 0.04s. The numeric core loss calculation of the magnetic link is done based on *Modified Steinmetz Equation* [27] and is found as 14.38 kW. The loss scenario is shown in Table III for the grid connected wind energy conversion system with the proposed OVM technique. This time, the switching losses are greater than the conduction loss as the converter operates for longer time in the linear

modulation region than in OVM region.

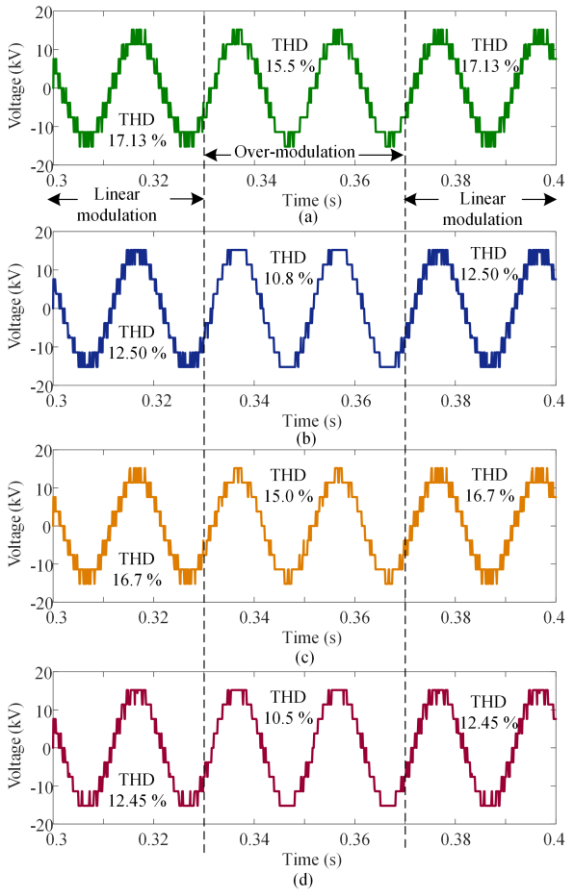

Fig. 13. Converter output voltage profiles with momentary OVM region for different modulation schemes: (a) SPWM, (b) THSDBCPWM, (c) SSDBCPWM, and (d) THPWM.

TABLE III
COMPARISONS OF REGULAR AND PROPOSED PDPWM IN GRID CONNECTED SYSTEM (OVM MODE EXISTS FOR 0.04 S)

Category PWM	Type	Switching loss (kW)	Conduction loss (kW)	Core loss (kW)	Total loss (kW)
SPWM	m = 1.8	15.14	2.67	14.38	32.19
	k = 0.4	12.01	2.50		28.89
SDBCPWM	m = 1.8	23.01	2.64		40.03
	k = 0.4	19.29	1.71		35.38
THPWM	m = 1.2	14.90	2.67		31.95
	k = 0.4	13.13	2.60		30.11
THSDBCPWM	m = 1.2	14.90	2.66		31.94
	k = 0.4	13.08	2.55		30.01

VII. EXPERIMENTAL RESULTS AND DISCUSSIONS

Experiments are conducted on the high-frequency magnetic-link based MLC in the islanded operation only for the validation of the performance of the converter in the OVM region. A laboratory prototype of 2.5 kVA, 600 V rated 5-level 3-phase converter system is developed with an LC filter. In this paper, a 2.5 kVA high-frequency toroidal magnetic core is developed with Metglas amorphous alloy ribbon 2605SA1 (the ribbon thickness of 20 µm and wide of 2.5 cm). Approximately, 0.96 kg ribbon is used. The core contains about 1000 layers with a volume of 133.52 cm^3. The core dimensions are 2.5 cm in height, and 6.5 cm and 10.5 cm in inner and outer diameters respectively. Fig. 14 shows a photograph of experimental setup. The primary winding of the magnetic-link is connected to a high-frequency full-bridge inverter fabricated with Semikron IGBT module SK30GH123. The gate pulses are generated with TMS320F28335 Delfino Microcontroller through driver SKHI 20opA to drive the CHB inverter for THPWM with the proposed OVM technique, as shown in Fig. 15. In comparison with the other modulation schemes, the THPWM scheme shows better performance in the proposed OVM technique and THPWM also simplifies the hardware implementation. Therefore, this modulation method is chosen to apply for the experimentation. The square wave input and output voltage of the magnetic link with rectified voltage from fast recovery diode DSEE15-12CC based rectifier and associated magnetizing current are exhibited in Fig. 16. The core loss scenario of the prototype core with the B-H curve is shown in Fig. 17 with 10 kHz square wave excitation generated with the high frequency inverter having 1.2 µs dead-band. The information found from the B-H curve of the core is crucial as it helps to understand the safe voltage or current handling capacity of the core, which prevents the magnetic core from saturation. The saturation mode is normally neglected as it draws huge current and excessively heats up the core. The dead-band effect on the core loss is demonstrated in the Fig. 17(b). With the carrier frequency of 3.15 kHz, the converter output line voltages and the corresponding current waveforms after filtering for the THPWM in the traditional and proposed OVM mode are shown in Fig. 18. It is found that the resultant THD value is slightly higher than that of the simulated value and the proposed technique shows better performance than existing OVM methods.

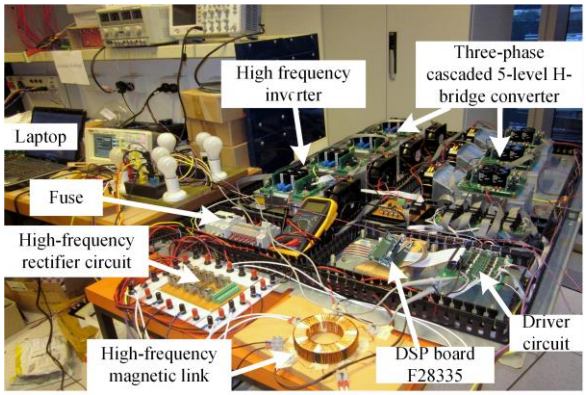

Fig. 14. A photograph of the experimental setup.

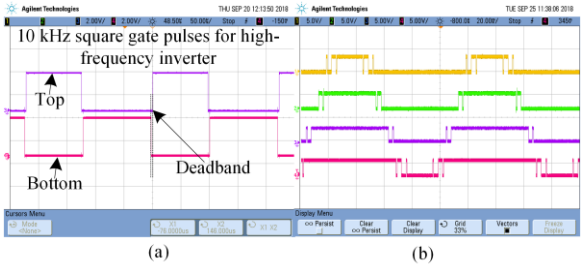

Fig. 15. (a) High-frequency gate pulses to drive high frequency inverter and (b) gate pulse generation from DSP F28335 for single phase voltage

generation of five-level CHB converter (proposed OVM with third harmonic injected signal).

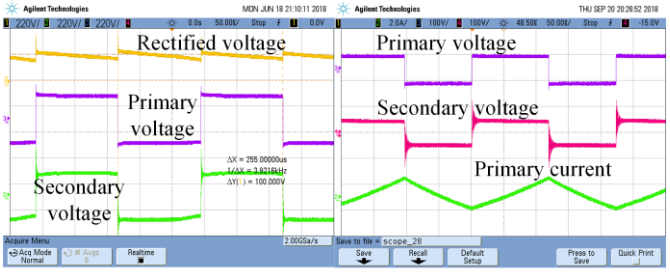

Fig. 16. (a) High-frequency magnetic link primary and secondary voltage with rectified output voltage and (b) primary and secondary voltage with corresponding magnetizing current.

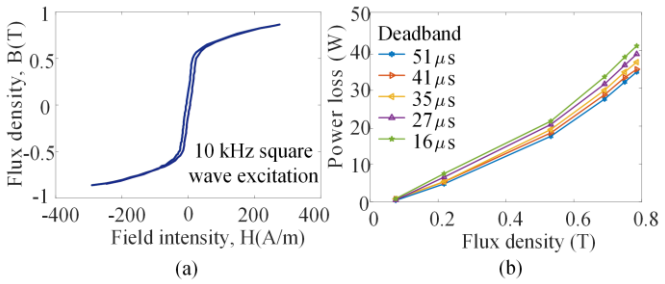

Fig. 17. (a) B-H loop of the core with high-frequency excitation with 1.2 μs dead-band and (b) core loss with 10 kHz square wave excitation.

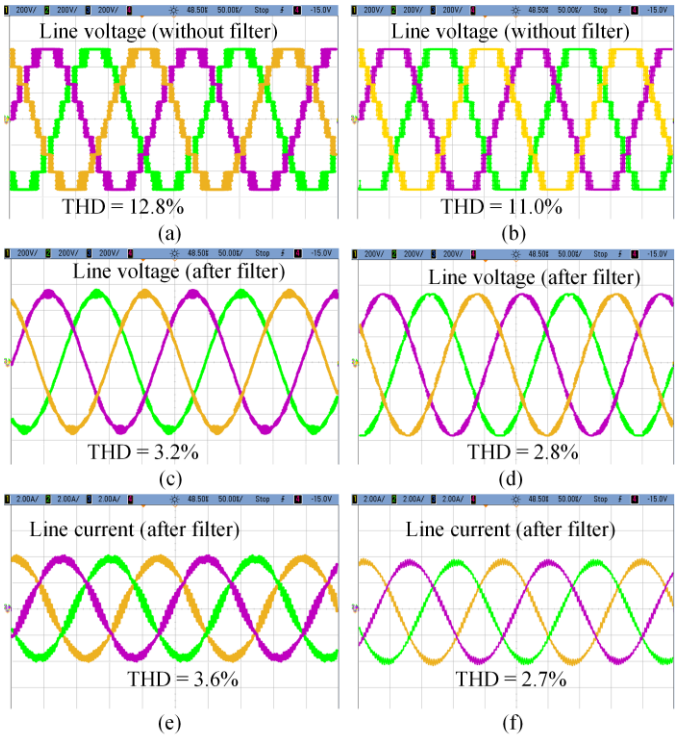

Fig. 18. Converter overall performance under existing (left column) and proposed (right column) OVM technique with third harmonic injected signal.

VIII. Conclusion

To improve the system performance, a modified OVM technique is presented in this paper with grid connected and islanded operation. With the proposed modified carrier signal based BCPWM techniques, the overall loss and THD are decreased for both the islanded and grid connected modes compared with those obtained by the traditional OVM techniques. Moreover, the voltage gain can be increased and remains approximately constant in the proposed method, which may not be possible to obtain using the traditional OVM methods. In this paper, a high-frequency magnetic link-based fully-rated CHB converter is developed for wind energy applications and the behavior of the system under rated and overrated load conditions are investigated. The use of magnetic link for the generation of isolated and balanced dc sources of the MLC inherently overcomes the voltage imbalance problem of CHB MLC and hence effectively simplifies the system control complexities. The core loss of high-frequency magnetic link is also measured to identify the overall loss of the system. The effectiveness of the proposed technology is confirmed by the simulation and experimental results.

References

[1] M. R. Islam, Y. G. Guo, J. G. Zhu, H. Lu, and J. X. Jin, "High-frequency magnetic-link medium-voltage converter for superconducting generator-based high-power density wind generation systems," *IEEE Trans. Appl. Supercond.*, vol. 24, no. 5, pp. 1–5, Oct. 2014.

[2] N. Mendis, K. M. Muttaqi, S. Perera, and S. Kamalasadan, "An effective power management strategy for a wind–diesel–hydrogen-based remote area power Supply System to meet fluctuating demands under generation uncertainty," *IEEE Trans. Ind. Appl.*, vol. 51, no. 2, pp. 1228–1238, Mar.–Apr. 2015.

[3] B. Jain, S. Jain, and R. K. Nema, "Control strategies of grid interfaced wind energy conversion system: An overview," *Renew. Sustain. Energy Rev.*, vol. 47, pp. 983–996, Apr. 2015.

[4] Y. Tan, K. M. Muttaqi, P. Ciufo, and L. Meegahapola, "Enhanced frequency response strategy for a PMSG-based wind energy conversion system using ultracapacitor in remote area power supply systems," *IEEE Trans. Ind. Appl.*, vol. 53, no. 1, pp. 549–558, Jan.–Feb. 2017.

[5] M. R. Islam, Y. G. Guo, and J. G. Zhu, "A multilevel medium-voltage inverter for step-up-transformer-less grid connection of photovoltaic power plants," *IEEE J. Photovolt.*, vol. 4, no. 3, pp. 881–889, May 2014.

[6] H. Abu-Rub, J. Holtz, J. Rodriguez, and G. Baoming, "Medium voltage multilevel converters—state of the art, challenges, and requirements in industrial applications," *IEEE Trans. Ind. Electron.*, vol. 57, no. 8, pp. 2581–2596, Aug. 2010.

[7] J. Lamb, B. Mirafzal, and F. Blaabjerg, "PWM common mode reference generation for maximizing the linear modulation region of CHB converters in islanded microgrids," *IEEE Trans. Ind. Electron.*, vol. 65, no. 7, pp. 5250–5259, Jul. 2018.

[8] Y. Yu, G. Konstantinou, B. Hredzak, and V. G. Agelidis, "Power balance optimization of cascaded H-bridge multilevel converters for large-scale photovoltaic integration," *IEEE Trans. Power Electron.*, vol. 31, no. 2, pp. 1108–1120, Feb. 2016.

[9] J. I. Leon, S. Kouro, S. Vazquez, R. Portillo, L. G. Franquelo, J. M. Carrasco, and J. Rodriguez, "Multidimensional modulation technique for cascaded multilevel converters," *IEEE Trans. Ind. Electron.*, vol. 58, no. 2, pp. 412–420, Feb. 2011.

[10] M. R. Islam, Y. G. Guo, and J. G. Zhu, "A high-frequency link multilevel cascaded medium-voltage converter for direct grid integration of renewable energy systems," *IEEE Trans. Power Electron.*, vol. 29, no. 8, pp. 4167–4182, Aug. 2014.

[11] A. R. Beig, "Synchronized SVPWM algorithm for the overmodulation region of a low switching frequency medium-voltage three-level VSI," *IEEE Trans. Ind. Electron.*, vol. 59, no. 12, pp. 4545–4554, Dec. 2012.

[12] M. Priestley, J. E. Fletcher, and C. Tan, "Space-vector PWM technique for five-phase open-end winding PMSM drive operating in the overmodulation region," *IEEE Trans. Ind. Electron.*, vol. 65, no. 9, pp. 6816–6827, Sep. 2018.

[13] P. D. Judge, G. Chaffey, M. M. C. Merlin, P. R. Clemow, and T. C. Green, "Dimensioning and modulation index selection for the hybrid

modular multilevel converter," *IEEE Trans. Power Electron.*, vol. 33, no. 5, pp. 3837–3851, May 2018.

[14] M. B. Ghat and A. Shukla, "A New H-Bridge Hybrid Modular Converter (HBHMC) for HVDC Application: Operating Modes, Control, and Voltage Balancing," *IEEE Trans. Power Electron.*, vol. 33, no. 8, pp. 6537–6554, Aug. 2018.

[15] P. D. Judge, G. Chaffey, M. M. C. Merlin, P. R. Clemow, and T. C. Green, "Dimensioning and modulation index selection for the hybrid modular multilevel converter," *IEEE Trans. Power Electron.*, vol. 33, no. 5, pp. 3837–3851, May 2018.

[16] S. Li, W. Chen, Y. Yan, T. Shi, and C. Xia, "A multimode space vector overmodulation strategy for ultrasparse matrix converter with improved fundamental voltage transfer ratio," *IEEE Trans. Power Electron.*, vol. 33, no. 8, pp. 6782–6793, Aug. 2018.

[17] Y. Xia, X. Zhang, M. Qiao, F. Yu, Y. Wei, and P. Zhu, "Research on a new indirect space-vector overmodulation strategy in matrix converter," *IEEE Trans. Ind. Electron.*, vol. 63, no. 2, pp. 1130–1141, Feb. 2016.

[18] K. Zhou and D. Wang, "Relationship between space-vector modulation and three-phase carrier-based PWM: a comprehensive analysis," *IEEE Trans. Ind. Electron.*, vol. 49, no. 1, pp. 186–196, Feb. 2002.

[19] M. R. Islam, A. M. M. Rahman, M. M. Islam, Y. G. Guo, and J. G. Zhu, "A modular medium voltage grid connected converter with improved switching techniques for solar photovoltaic systems," *IEEE Trans. Ind. Electron.*, vol. 64, no. 11, pp. 8887–8896, Nov. 2017.

[20] S. K. Giri, S. Mukherjee, S. Kundu, S. Banerjee, and C. Chakraborty, "An improved PWM scheme for three-level inverter extending operation into overmodulation region with neutral-point voltage balancing for full power-factor range," *IEEE J. Emerg. Sel. Topics Power Electron.*, vol. 6, no. 3, pp. 1527–1539, Sep. 2018.

[21] W. Lin, D. Jovcic, S. Nguefeu, and H. Saad, "Full-bridge MMC converter optimal design to HVDC operational requirements," *IEEE Trans. Power Del.*, vol. 31, no. 3, pp. 1342–1350, Jun. 2016.

[22] M. Jankovic, A. Costabeber, A. Watson, and J. C. Clare, "Arm-balancing control and experimental validation of a grid-connected MMC with pulsed DC load," *IEEE Trans. Ind. Electron.*, vol. 64, no. 12, pp. 9180–9190, Dec. 2017.

[23] R. Picas, S. Ceballos, J. Pou, J. Zaragoza, G. Konstantinou, and V. G. Agelidis, "Closed-loop discontinuous modulation technique for capacitor voltage ripples and switching losses reduction in modular multilevel converters," *IEEE Trans. Power Electron.*, vol. 30, no. 9, pp. 4714–4725, Sep. 2015.

[24] X. Li, Q. Song, W. Liu, Q. Li, H. Rao, and S. Xu, "Zero-sequence voltage injection control scheme of modular multilevel converter supplying passive networks under unbalanced load conditions," *J. Elect. Power Syst. Research*, vol. 121, pp. 270–278, Apr. 2015.

[25] M. A. Rahman, M. R. Islam, Youguang Guo, Jianguo Zhuy, and Gang Lei, "Modified carrier-based over-modulation technique for improved switching performance of multilevel converters," In Proc. *20th Int. Conf. Elect. Mach. Syst.*, 11–14 Aug. 2017, Sydney, NSW, Australia, pp. 1–6.

[26] S. R. Pulikanti, K. Muttaqi, and D. Suntanto, "Control of five-level flying capacitor based active-neutral-point-clamped converter for grid connected wind energy applications," In Proc. *2012 IEEE Ind. Appl. Society Annual Meeting*, 7–11 Oct. 2012, Las Vegas, NV, USA, pp. 1–9.

[27] J. Reinert, A. Brockmeyer, and R. W. A. A. De Doncker, "Accurate calculation of losses in ferro- and ferrimagnetic materials based on the modified Steinmetz equation," *IEEE Trans. Ind. Appl*., vol. 37, no. 4, pp. 1055–1060, Jul./Aug. 2001.